Transport in Porous Media (2021) 138:611–636
https://doi.org/10.1007/s11242-021-01634-x

Flow and Transport Properties of Deforming Porous Media. II. Electrical Conductivity

Samuel Richesson[1] · **Muhammad Sahimi**[1]

Received: 16 February 2021 / Accepted: 30 May 2021 / Published online: 7 June 2021

Abstract
In Part I of this series, we presented a new theoretical approach for computing the effective permeability of porous media that are under deformation by a hydrostatic pressure P. Beginning with the initial pore-size distribution (PSD) of a porous medium before deformation and given the Young's modulus and Poisson's ratio of its grains, the model used an extension of the Hertz–Mindlin theory of contact between grains to compute the new PSD that results from applying the pressure P to the medium and utilized the updated PSD in the effective-medium approximation (EMA) to estimate the effective permeability. In the present paper, we extend the theory in order to compute the electrical conductivity of the same porous media that are saturated by brine. We account for the possible contribution of surface conduction, in order to estimate the electrical conductivity of brine-saturated porous media. We then utilize the theory to update the PSD and, hence, the pore-conductance distribution, which is then used in the EMA to predict the pressure dependence of the electrical conductivity. Comparison between the predictions and experimental data for twenty-six sandstones indicates agreement between the two that ranges from excellent to good.

Keywords Porous media · Hydrostatic pressure · Deformation · Formation factor · Effective-medium approximation

1 Introduction

This paper is the second part in a series devoted to theoretical analysis and computation of flow and transport properties of porous media that undergo deformation as a result of applying an external force or hydrostatic pressure. In the previous paper (Richesson and Sahimi under review), hereafter referred to as Part I, we analyzed the problem of estimating the effective permeability K_e of deforming porous media and presented a new formulation of the problem based on a modified Hertz–Mindlin theory of contacting grain (Hertz 1882; Mindlin 1949) and the effective-medium approximation (EMA) for transport properties of

✉ Muhammad Sahimi
moe@usc.edu

[1] Mork Family Department of Chemical Engineering and Materials Science, University of Southern California, Los Angeles, CA 90089-1211, USA

heterogeneous materials. We demonstrated that the new formulation provides accurate estimates of K_e by comparing its predictions with a large set of experimental data for a variety of sandstones. In the present paper, we analyze the problem of predicting the electrical conductivity of brine-saturated porous media and, in particular, in the same sandstones.

As is well known, in most porous materials, both natural and synthetic, pores have complex shapes; they are interconnected with their connectivity being stochastically distributed and forming tortuous flow and transport paths. Characterization of such porous media has always been a problem of fundamental importance and has been studied for a long time. One way of gaining information on the structure of a pore space is by relating its flow and transport properties to the quantities that shed light on its morphology. In particular, consider a porous medium that is saturated by brine with electrical conductivity σ_f. If the effective conductivity of the saturated medium is σ_e, then

$$F = \frac{\sigma_f}{\sigma_e} , \tag{1}$$

where F, the formation factor, is a geometrical characteristic of the pore space. In the limit of long times, the effective diffusion coefficient of a molecule probing the same pore space is given by

$$D_e = \frac{D_0}{F\phi} , \tag{2}$$

where ϕ is the porosity of the porous medium, and D_0 is the free diffusion coefficient outside the pore space. It is, therefore, clear that measurements of D_e and σ_e, or the ability to accurately predict them, provide valuable information on the morphology of the pore space (see, for example, Vanderborght et al. 2005; Crook et al. 2008; Ghanbarian and Berg 2017). Thus, in addition to numerous measurements of the diffusivity and electrical conductivity of a wide variety of porous media, various theoretical approaches have also been developed for predicting σ_e and D_e, beginning with Archie (1942) and Wyllie and Spangler (1952), and continuing with Woessner (1963); Stejskal and Tanner (1965), and Karger et al. (1981), all the way to the present time (Ghanbarian et al. 2014; Dashtian et al. 2015); for a review, see Cai et al. (2017). Moreover, short-time behavior of D_e, before it reaches its asymptotic value given by Eq. (2), has been linked with the ratio of surface S_p of the pores and their volume V_p, and has been exploited fruitfully to make progress on the general problem of characterizing a porous medium (Mitra and Sen 1992; Mitra et al. 1992a, 1993).

Almost all the progress that has been made over the past several decades relates to the electrical conductivity and diffusivity of *rigid* porous media. As discussed in Part I, flow and transport properties of porous media that deform as a result of being subjected to an external driving potential, either pressure or force, are also important and appear in many problems of fundamental scientific importance, as well as practical applications, particularly in characterization of laboratory-scale porous media, as well as gaining information about the structure of field-scale porous media through their resistivity logs.

In the present paper, we study the problem of the pressure dependence of the static electrical conductivity of the brine-saturated porous media. Woodruff et al. (2015) developed an experimental approach for simultaneous measurement of the stress dependence of ultrasonic wave velocities and the components of the elastic stiffness and of the complex conductivity tensors over a wide range of frequency, from 100 mHz to 10 Hz. Their data indicated strong stress dependence of the ultrasonic and complex conductivity measurements,

which they attributed to the opening and closing of cracks within the samples. In a more recent paper, Revil et al. (2019) reported extensive experimental data for the effect of the pressure on the complex conductivity of five sandstone core samples from outcrops, as well as a sandstone analog that they had constructed using sintered glass beads. Their data may be analyzed by a method similar to what we describe in the present paper, except that one must use the EMA for frequency-dependent conductivity of heterogeneous materials (Odagaki and Lax 1981; Sahimi et al. 1983); see Sahimi (2003) for a comprehensive discussion).

The rest of this paper is organized as follows: In Sect. 2, we summarize the new theoretical approach to determining the change in the size of the pores when a hydrostatic pressure P is applied to a porous medium. The theory is then used in Sect. 3 to determine the evolution of the pore-conductance distribution (PCD) during deformation. Section 4 describes the EMA for estimating the effective electrical conductivity of brine-saturated porous media. In Sect. 5, we describe how to estimate the contribution of surface conduction to the total conductivity of the pore space. Since the proposed theory involves three parameters, Sect. 6 describes their estimation. The computational procedure is described in Sect. 7, while Sect. 8 presents the theoretical predictions for the electrical conductivity of a wide variety of sandstones and compares them with the experimental data. Section 9 discusses a few aspects of the theoretical approach and its limitations, while the paper is summarized in Sect. 10.

2 Mean-Field Theory of Deformation of Porous Media under a Hydrostatic Pressure

As mentioned in Introduction, we employ the EMA to predict the effective electrical conductivity of porous media that deform as a result of applying an external force or hydrostatic pressure. The EMA represents a type of mean-field approximation (MFA) that replaces a heterogeneous porous medium by an uniform one in which all the pores have the same effective size r_e. Deriving the solution of the flow or transport problem in the uniform system is straightforward. Then, the radius r_e of a randomly selected pore in the effective medium is replaced by its actual value in the original heterogeneous pore space, with the remaining pores still having the same size r_e. The replacement gives rise to perturbation in the solution of the uniform porous medium, whose magnitude is the difference between the solution for the uniform medium and one that is uniform everywhere, except in that one pore. Since the single pore is selected at random and its actual size follows the pore-size distribution (PSD) of the pore space, one sets to zero the average of the perturbation, with the averaging taken over the PSD. In effect, what the EMA does is transforming a multibody system into a one-body problem by accounting for the interaction of only a single pore with the rest of the effective medium. The effect of the remaining part of the disordered porous medium is represented by the far-field external pressure or potential gradient applied to the porous medium for inducing fluid flow or transport.

In the spirit of the EMA, and in order to develop a tractable theoretical approach consistent with the mean-field nature of the EMA, we considered in Part I the interaction between only two grains and its influence on the pore between the two, subject to an external force F or the corresponding hydrostatic pressure P applied to the porous medium. We then derived a formulation for determining how the deformation of the pore space changes the size of pore between the two grains. Similar to the EMA, the effect of the deformation

of the rest of the pore space was represented by the far-field applied pressure P or force F. The applied pressure P changes the PSD of the pore space, which in turn alters its effective permeability and electrical conductivity. The input to the EMA is the PSD or (PCD) of the pore space. Therefore, if the change in the PSD or PCD as a result of applying a pressure or force to the pore space is determined, the EMA may be used to estimate the effective permeability K_e and electrical conductivity σ_e of the porous medium at that pressure. In Part I, the idea was developed for computing K_e. In the present paper, we further extend the theory in order to compute σ_e.

Since the equation that describes the change in the PSD of a porous medium as a result of applying a hydrostatic pressure P was derived in Part I, we only present the final result here and refer the interested reader to Part I for complete details. In Part I, we showed that by applying a hydrostatic pressure to a porous medium, the closest distance between the surfaces of the aforementioned two grains decreases by u, given by

$$u = R_g \left(\frac{R_g}{R}\right)^{1/3} \left[\frac{3P(1-\nu^2)}{E_e}\right]^{2/3}, \tag{3}$$

where E_e, R_g, R, and ν are, respectively, the effective Young's modulus, radius, radius of curvature, and the Poisson's ratio of the grains. If the grains are roughly spherical, then $R_g \approx R$, which we assume to be the case or that, at the minimum, we can define an effective radius for an equivalent spherical particle.

3 Evolution of Pore-Size and Pore-Conductance Distributions as Functions of the Hydrostatic Pressure

Since the MFA neglects the interactions of two neighboring grains with other grains, the pore between them does not also interact with the pores farther away. Therefore, to a first-order approximation, the effective radius of the pore between two grains in a porous medium under an external hydrostatic pressure P decreases by $u/2$, where u is given by Eq. (3). In other words, the initial PSD distribution $f_0(r_0)$ before any pressure is applied is transformed to a new PSD $f_P(r_P)$ at pressure P where $r_P = r_0 - u/2$. If $f_0(r_0)$ is given, either analytically or numerically, then, since, $f_P(r_P) = f_0(r_0 - u/2)$, one either has an analytical expression for $f_P(r_P)$, or constructs it numerically for any pressure P.

Suppose that σ_P is the conductance of a pore when the pore space is under the pressure P. Then, since $\sigma_P \propto r_P^2$, given a PSD $f_P(r_P)$, one obtains the PCD by $h_P(\sigma_P)d\sigma_P = f_P(r_P)dr_P$. That is, for any pressure P, the PSD $f_P(r_P)$, updated by using Eq. (3), yields the corresponding PCD $h_P(\sigma_P)$, which is then used in the EMA in order to determine the effective electrical conductivity σ_e of the porous medium.

4 Effective-Medium Approximation for the Effective Conductivity

The morphology of any porous medium consists of pore throats that are connected together via the pore bodies. The effective sizes of both pore throats and pore bodies are distributed according to statistical distributions $f_t(r_t)$ and $f_b(r_b)$. But, whereas experimental measurement of $f_t(r_t)$ is straightforward (see, for example, Sahimi 2011; Blunt 2017 for discussions of various measurement methods), measuring $f_b(r_b)$ is not

straightforward. On the other hand, both macroscopic permeability and electrical conductivity of porous media are controlled by the pore throats, which, for convenience, are referred to as pores, and their distribution $f(r)$ as the PSD. Since in the EMA a heterogeneous pore space is represented by a uniform medium in which the size of all the pores is r_e, which we assume to be cylindrical, then its electrical conductivity is, $\sigma_P \propto r_P^2$. One can, of course, consider other pore shapes. The EMA predicts that the macroscopic electrical conductivity σ_e is given by Doyen (1988); David et al. (1990)

$$\sigma_e = \left(\frac{\phi}{\tau} \frac{r_e^2}{\langle r_b^2 \rangle} \right) \sigma_f \,, \tag{4}$$

where ϕ is the porosity, and τ is the tortuosity for which various theories, as well as empirical and semi-empirical relations, have been developed (for a review, see Ghanbarian-Alavijeh et al. 2013). Since the distribution $f_b(r_b)$ of the size of the pore bodies is typically not available, David et al. (1990) suggested that one should use,

$$\langle r_b^2 \rangle \simeq \langle r^2 \rangle = \int_{r_m}^{r_M} r^2 f(r) dr \,, \tag{5}$$

with r_m and r_M being, respectively, the minimum and maximum pore radii. We assume the same in this paper. In the EMA, an effective conductance g_e is computed by

$$\int_{g_m}^{g_M} \frac{g_e - g}{g + (D-1)g_e} h(g) dg = 0 \,. \tag{6}$$

Here, g_e and g_M are, respectively, the minimum and maximum conductances, D is the dimensionality of space ($D = 3$), and $h(g)$ is the pore-conductance distribution. Since $g_e \propto r_e^2$, $g \propto r^2$, and $h(g)dg = f(r)dr$, so that $h(g) = f(r^2)dr/dg = f(r^2)(1/2r)$, we obtain an alternative formulation directly in terms of $f(r)$:

$$\int_{r_m^2}^{r_M^2} \frac{r_e^2 - r^2}{r^2 + (D-1)r_e^2} \frac{f(r^2)}{2r} dr = 0 \,. \tag{7}$$

As for the tortuosity factor τ, we used $\tau = \phi^{1-m}$. The review by Ghabbarian et al. (2013) indicates that $1.2 \le m \le 4.4$ for a wide variety of porous media. After some preliminary simulations by which we tested the accuracy of various values of m, we set $m = 4$, which is for tortuous porous media.

Mukhopadhyay and Sahimi (2000) derived an EMA for predicting direction-dependent macroscopic conductivity of anisotropic porous media, while Stroud (1975) presented a continuum EMA for anisotropic media in which the local conductivity was a tensor. Other applications of the EMA were pointed out in Part I, to which the interested reader is referred.

5 Accounting for Surface Conduction

The experimental data for the electrical conductivity of porous media that we compare with the predictions of the model are in terms of the formation resistivity factor F, reported by Yale (1984). Equation (1) that defines F is based on the effective conductivity of the saturated pore space and does not include possible contribution by conduction across the pores' surface. Depending on the chemical composition of a porous medium, however, particularly in a clay-bearing one, surface conduction may contribute significantly to the overall measured conductivity, since the clay grains' surface allows for a layer of counterions that facilitates the development of a significant negative surface charge (Waxman and Smits 1968; Clavier et al. 1984). In fact, Revil et al. (2019) reported that the conductivity of the sandstones that they measured was dominated by their surface conductivity, since pore water salinity was low in their experiments. They interpreted their data using the Stern layer polarization model (Stern 1924). The Stern layer represents the inner part of the electrical double layer that coats the grains' surface. The data reported by Yale (1984) are for a broad variety of sandstones, which do have significant clay content (see also below). Therefore, it is imperative to account for surface conduction, before comparing the predictions of the theory, which does not take into account the effect of surface conduction, with the data.

Revil et al. (1998) derived the following equation for the total conductivity σ_t of a pore space, including the contribution by surface conductivity, which is saturated by a fluid with a pH between 5 and 8:

$$\sigma_t = \left(\frac{\sigma_f}{F}\right)\left\{1 - t^f_{(+)} + F\xi + \frac{1}{2}\left(t^f_{(+)} - \xi\right)\left[1 - \frac{\xi}{t^f_{(+)}} + \sqrt{\left(1 - \frac{\xi}{t^f_{(+)}}\right)^2 + \frac{4F\xi}{t^f_{(+)}}}\right]\right\}, \quad (8)$$

where $t^f_{(+)}$ is the Hittorf transport number of cations in the free electrolyte (brine in pores), and ξ is known as the *Dukhin number* (Lyklema 1993), which is the ratio of surface and fluid conductivities. Equation (8) reduces to Eq. (1) in the limit $\xi \to 0$. The brine used in the experiments of Yale (1984) was NaCl, for which $t^f_{(+)} \approx 0.38$. Thus, if the second parameter of Eq. (8), namely ξ, is also known, then, for every measured σ_t one can use it to compute the corresponding formation factor F.

Revil et al. (1998) derived the following equation for the Dukhin number,

$$\xi = \frac{2\rho_g C\beta}{3\sigma_f}. \quad (9)$$

Here, ρ_g is the density of the solid matrix, C is the cation exchange capacity, and β is the equivalent mobility for surface conduction. Equation (9) provided accurate predictions for clay-rich sediments (Daigle et al. 2015). Because the grains' density and the exact chemical compositions of the sandstones that we consider were not given by Yale (1984), we cannot determine the Dukhin number for them. Thus, since ξ is independent of the hydrostatic pressure, we use one data point for the conductivity of every sandstone that we consider in order to estimate the Dukhin number using the above equation. This point was selected in the middle of the experimental pressure range.

6 Computational Procedure

Given the theoretical formulation for predicting the effective electrical conductivity σ_e of deforming porous media, the following computational procedure was used to calculate σ_e.

1. Given the initial PSD $f_0(r_0)$ and, therefore, an initial conductance distribution $h_0(g_0)$ of an undeformed porous medium, its electrical conductivity was computed using Eqs. (4), (5), and (7).
2. For a given hydrostatic pressure P, the corresponding PSD $f_P(r_P)$ was constructed by selecting the pore sizes from $f_0(r_0)$, calculating their updated values using Eq. (1) and $r_P = r_0 - u/2$, and repeating it for a large number of pore sizes selected from $f_0(r_0)$, so that an accurate $f_P(r_P)$ was obtained.
3. The PSD $f_P(r_P)$ and Eq. (5) were then utilized to determine $\langle r_b^2(P)\rangle = \langle r_P^2\rangle$. The result was used together with $f_P(r_P)$ in Eqs. (4) and (7) to compute $\sigma_e(P)$ at pressure P.
4. To compare the predictions in (3) with the experimental data for a given porous medium, we utilized the experimental value of the total conductivity σ_t on the left side of Eq. (8) at a single pressure and determined the parameter ξ, using as the formation factor F its theoretical prediction. In effect, for every sandstone we used a single experimental point to estimate ξ. Since ξ is independent of P, we used the same estimate in Eq. (8) and solved for the formation factor F at various pressures P, given that the left side of Eq. (8) is the experimental value of the total conductivity.
5. The resulting values of F at various pressures P represent the true values of the formation factor over the pressure range for a given porous medium, which are then compared with the theoretical predictions.

Note that if all the parameters of Eq. (9) are known, it can be utilized to estimate ξ directly, without any need for step (4). In that case, the estimate of ξ and the experimental data for σ_t for a given porous medium are used directly in Eq. (8) and the resulting nonlinear equation is solved numerically for the true formation factors F. Note also that if the PSD $f_0(r_0)$ is expressed by an analytical expression, $f_P(r_P)$ will also be determined analytically, in which case the computations will be very fast.

7 The Parameters of the Model

The parameters of the model are the Poisson's ratio ν and the Young's modulus E_e of the grains (not the porous medium) that appear in Eq. (3), the PSD, and the Dukhin number ξ. If experimental data for the parameters are available, they can be used directly in the theory, but they are not available for the sandstones that we analyze.

We already described how we estimate ξ. As discussed in Part I, the predictions of the model are sensitive to the value of the Young's modulus. In Part I, we explained how we estimate E_e. Since the experimental data that we compare with the theoretical predictions are for the same sandstones as those in Part I, we use the same values of E_e.

As for the Poisson's ratio, in Part I we demonstrated that if all the parameters but ν are fixed, the Poisson's ratio is varied by a factor of 4, and the model is used to predict the dependence on the applied pressure of the permeability of the sandstones, the predictions

vary by at most 2 percent. Thus, we fix the Poisson's ratio at $\nu \approx 0.3$, the same value that we used in Part I, which is in the middle of the range reported for sandstones.

The sensitivity of the predictions to the PSD was also studied in Part I. To do so, we used the following theoretical PSD distribution,

$$f(r) = \left[\frac{r - r_{\rm m}}{(r_0 - r_{\rm m})^2}\right] \exp\left[-\frac{1}{2}\left(\frac{r - r_{\rm m}}{r_0 - r_{\rm m}}\right)^2\right], \tag{10}$$

where r_0 is a parameter related to the average pore size $r_{\rm a}$ through $r_{\rm a} = (r_0 r_{\rm m})\sqrt{pi/2} + r_{\rm m}$. We held the minimum pore size $r_{\rm m}$ constant at 0.18 μm, the lowest pore sizes that we identified in the published PSDs for sandstones and varied r_0 over about two orders of magnitude. Figure 1a presents the PSD that Eq. (10) generates. The distribution corresponding to the lowest r_0 in Fig. 1a is completely similar to the PSD reported by Fredrich et al. (1993) for a Fontainebleau sandstone, while those generated by other values of r_0 are qualitatively similar to those reported by others for other types of sandstone. As we demonstrated in Part I, the predicted effective pressure-dependent permeabilities of the sandstones that we analyzed in Part I were not greatly sensitive to the PSD. Therefore, similar to Part I, in the absence of any experimental data for each of the PSDs of the sandstones that we analyze below, we used in all cases described below the distribution presented in Fig. 1b as the initial PSD, $f_0(r_0)$, which was reported by Lindquist et al. (2000) for a Fontainebleau sandstone, which is also similar qualitatively to those for many other sandstones reported by others (see, for example, Cheung et al. 2012 for the Bleurswiller and Boise sandstones).

Table 1 summarizes the parameters $E_{\rm e}$ and ξ, as well as the initial porosity ϕ_0 of all the sandstone that we analyze in the following section.

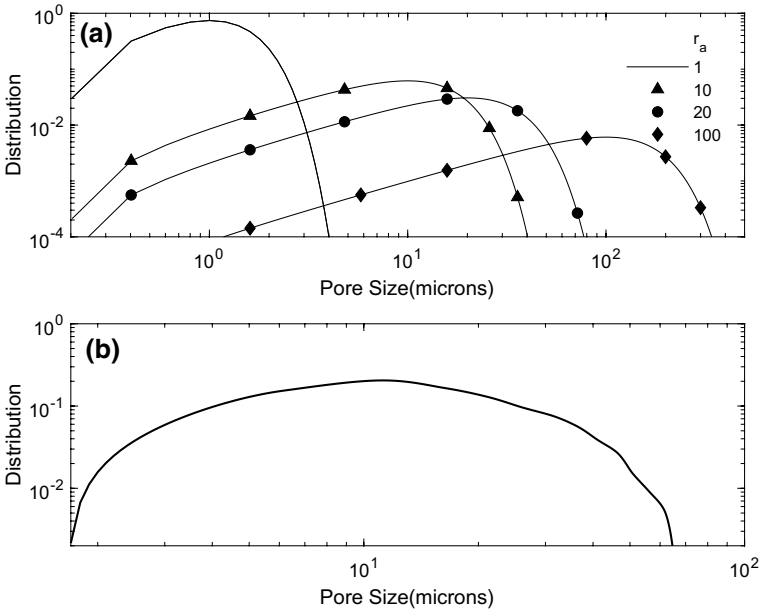

Fig. 1 **a** The PSDs generated by Eq. (10) for various average pore sizes $r_{\rm a}$. **b** The PSD used in all the calculations

Table 1 Estimates of the Young's modulus E_e (in GPa), the initial porosity ϕ_0, and the Dukhin number ξ of the sandstones

Sandstone	E_e	ϕ_0	$\xi \times 10^3$	Sandstone	E_e	ϕ_0	$\xi \times 10^3$
Fontainebleau	40	0.052	0.0	Beaver	2.7	0.076	3.3
Berea 100H	25	0.165	18.9	Berea 500	13	0.2	2.6
Boise	38.5	0.26	16.2	Cambrian 6	10	0.08	2.3
Cambrian 14	12	0.11	6.1	Cambrian 16	2	0.13	1.3
Fahler 142	0.12	0.08	4	Fahler 154	0.15	0.044	3.4
Fahler 162	0.11	0.03	1.3	Fahler 189	0.17	0.02	≈ 0.0
Indiana DH	30	0.27	49.5	Massillon DH	9.5	0.161	17.3
Miocene 7	5	0.083	1.2	Pliocene 35	4	0.2	4.1
Tensleep	2.6	0.146	29.6	Gulf Coast	6.4	0.22	22.7
Torpedo	3	0.202	8.6	Triassic 26	8	0.18	31.6
Triassic 27	6.5	0.18	29.9	Triassic 34	83	0.2	37.1
Triassic 38	40	0.2	33.1	Triassic 41	2.8	0.21	3.3
Branford	0.7	0.11	4.2	Kirkwood	0.5	0.13–0.18	12.7

8 Theoretical Predictions and Comparison with Experimental Data

Before we present the predictions of the theory and compare them with the experimental data; three points are worth mentioning.

1. First, we emphasize that the model presented in Sects. 2–5 is a MFA that, similar to any MFA, neglects the fluctuations in the local properties, hence making it possible to analyze the behavior of a heterogeneous porous medium based on only a single pore between two grains, the minimum number for a meaningful analysis. This also implies that only an average grain size is required. As such, similar to all the MFAs, the approach has its limitations and strengths.
2. Second, for at least some of the sandstones that we analyze below, if we plot $\sigma_e(P)/\sigma_e(0)$ versus a suitably selected rescaled P, we obtain a more or less single universal master curve. The master curve represents essentially the dimensionless response of the porous media under study to the changes in the pressure, since the initial PSD, the Poisson's ratio, and the exponent m are all set to constant values. A clue to the proper rescaling of P is provided by Eq. (3), since it implies that the quantity u/R_g is a function only of P/E_e.

   The existence of such a master curve implies that it can predict the measurements by rescaling the pressure axis to generate a dimensionless form based on the input data—the initial porosity and an experimental data point that provides an estimate for the effective Young's modulus E_e. Other mechanical models than the HM theory of point contact may provide a different master curve. A master curve for another important property of large-scale porous media was proposed by Rassamdana et al. (1996).
3. We point out that, in principle, there is no rigorous theoretical relation between the permeability—essentially the square of a relevant length scale of a pore space and, hence, a static property—and electrical conductivity, which is a dynamic property. Therefore, aside from their sharing the same flow and transport paths, one cannot necessarily draw any conclusion for one based on the behavior of the other one. This is particularly true

for porous media, such as the almost all the sandstones that we analyze, which contain a significant volume fraction of clays, and therefore, surface conduction may play a significant role in electrical conduction.

We used the theory to predict the pressure dependence of the effective electrical conductivity $\sigma_e(P)$ of a large number of sandstones and to compare the predictions with the experimental data, almost all of which are given by Yale (1984). He did not provide the sandstones' initial PSD, and therefore, as mentioned earlier, we used in all the cases described below the PSD presented in Fig. 1b. In Part I, we described the geological characteristics of each sandstone, and therefore, they will not be repeated here.

Yale (1984) stated that in all the cases that he experimented on, the pore pressure P_P was constant. Thus, in what follows the pressure P may be replaced by $P - P_P$.

8.1 Fontainebleau Sandstone

We first present the predictions for a Fontainebleau sandstone, for which Farid (2016) reported measurements of the pressure dependence of its conductivity. The initial porosity ϕ_0 of the sandstone, before deformation, was 0.052. Farid (2016) also stated that the clay content of the sandstone was negligible. Therefore, we took the Dukhin number $\xi = 0$. Figure 2 compares the predictions, normalized by the initial conductivity, with the experimental data. Note that since $\xi = 0$, no fitting parameter was used. The agreement between the two sets is very good, with the maximum difference being no more than 7 percent.

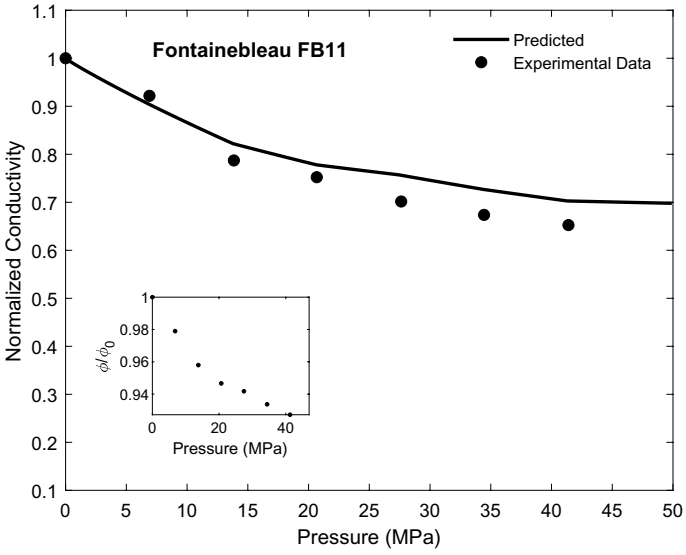

Fig. 2 Comparison of the predicted conductivities with the experimental data for the Fontainebleau sandstone

8.2 Beaver River Sandstone

The Beaver River sandstone is a formation on the west side of the Athabasca River near Mildred Lake and the Beaver River (in Alberta, Canada), with an initial porosity (before deformation) of $\phi_0 \approx 0.076$. Figure 3 compares the predicted pressure dependence of the sandstone's electrical conductivity, normalized by its value before deformation, with the experimental data of Yale (1984) who also presented all of his data in normalized fashion. The agreement between the two is excellent, with the largest difference between the predictions and the data being about 8 percent at the highest pressure.

We note that, at high pressures, there is a qualitative difference between the dependence of the conductivity of the Beaver sandstone and its permeability, shown in Fig. 6 of Part I. The theory predicts faster decay of the conductivity than the experimental data, whereas its predictions for the permeability are highly accurate at all pressures. This may be due to the inadequacy of Eq. (8) for accounting for the effect of surface conduction; the inadequacy of the way we accounted for it by fitting the parameter ξ to a single data point, or both, since slower decay of the conductivity, and the absence of the same trends in the permeability clearly point toward the significance of surface conduction.

8.3 Berea Sandstones

The electrical conductivities of two Berea sandstones were reported by Yale (1984). One was Berea 100H, a sandstone whose bedding was horizontal, with an initial porosity of 0.165. Figure 4 compares the predictions with the experimental data. Although the maximum difference between the predictions and the data is about 2.5 percent, the theory predicts continuous decline of the conductivity with increasing pressure, whereas the experimental data indicate that at the highest pressures the conductivity levels off,

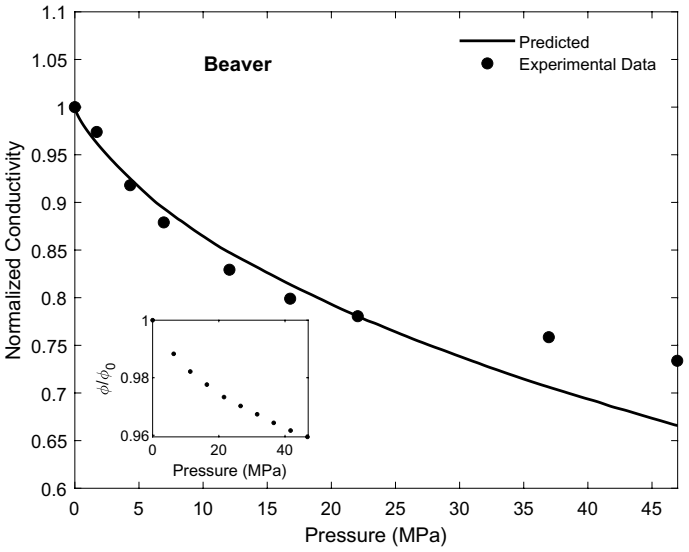

Fig. 3 Comparison of the predicted conductivities with the experimental data for the Beaver sandstone

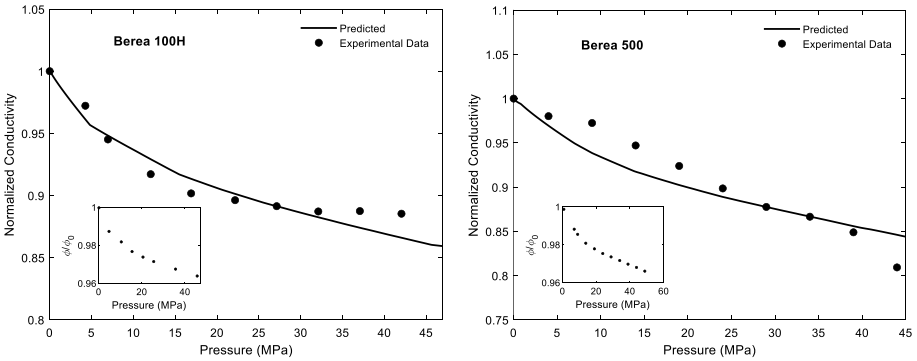

Fig. 4 Comparison of the predicted conductivities with the experimental data for two Berea sandstones

hence indicating that either the morphology of the sandstone did not change at the highest pressure, or we did not account for the effect of surface conduction properly.

Berea 500, with an initial porosity of 0.2, was the second sandstone whose conductivity was reported by Yale (1984). Figure 4 also compares the predictions with the experimental data with the same level of accuracy as the predictions for Berea 100H, except that in this case the measured electrical conductivity decays a bit faster than the predictions at the highest pressures.

A clue to this is obtained from Fig. 8 of Part I in which we compare the theoretical predictions with the experimental data for the permeability of the same sandstones. That figure indicates excellent agreement between the predictions and the data at all the pressures. Since the porous media in both cases are the same, it may imply that the model may underestimate the contribution of surface conduction in case of Berea 100H, but overestimates it in the case of Berea 500.

8.4 Boise Sandstone

The Boise sandstone had an initial porosity of 0.26. Figure 5 compares the predictions with the experimental data. At lower pressures, the measured electrical conductivity seems to decay a bit faster than the predictions, while the opposite trends develop at the highest pressures. Note, however, that the percentage difference between the two sets is no more than 4 percent, well within the measurements' uncertainties.

8.5 Cambrian Sandstone

Cambrian sandstones are low-porosity formations from the Cambrian era. Yale reported their electrical conductivity for three samples, referred to as Cambrian 6, 14, and 16, with initial porosities of 0.08, 0.11, and 0.13, respectively. Figure 6 compares the predicted pressure dependence of the effective conductivity with the experimental data. In all cases, the agreement between the predictions and the data is excellent.

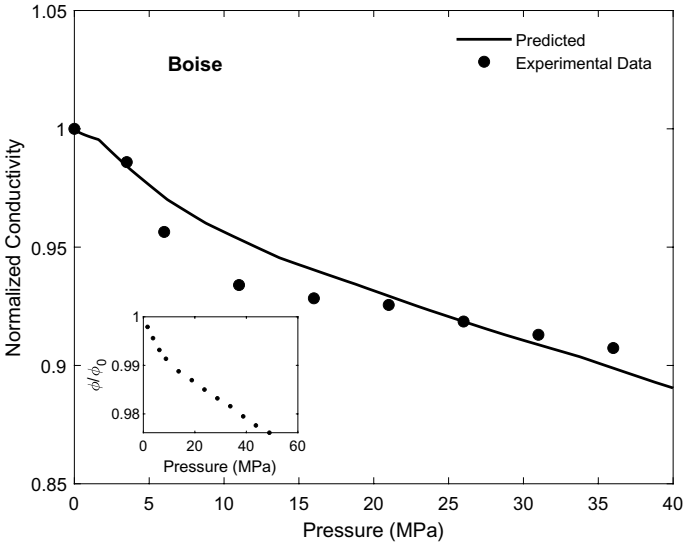

Fig. 5 Comparison of the predicted conductivities with the experimental data for the Boise sandstone

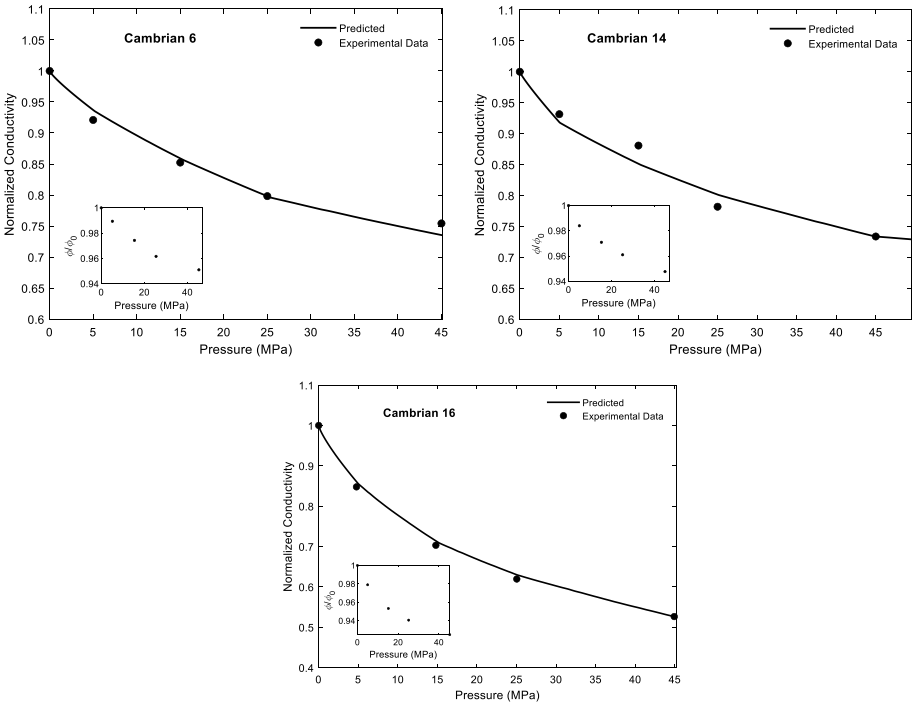

Fig. 6 Comparison of the predicted conductivities with the experimental data for the three Cambrian sandstones

8.6 Fahler Sandstones

Pressure dependence of the electrical conductivities of four samples of Fahler sandstones, from Fahler strata in Spirit River formation (in Grande Cache in Alberta, Canada), were reported by Yale (1984). They were referred to as Fahler 142, 154, 162, and 189, with their geological characteristics described in Part I. Their initial porosities were, respectively, $\phi_0 \approx 0.08,\ 0.044,\ 0.03$, and 0.02. Figure 7 compares the predictions with the experimental data, with the agreement between the two being generally excellent for three of the sandstones, namely Fahler 142, 154, and 189.

In the case of Fahler 162, the agreement between the data and the predictions is good at higher pressures, but the difference between the two sets for the three smallest pressures is relatively large, although their trends are completely similar. Note that, among the four Fahler sandstones, the largest deformation-induced decline in the porosity belongs to Fahler 162, whose porosity was reduced by about 20 percent over the intermediate values of the applied pressure. Given that the initial porosity of the sandstone was only 0.03, its corresponding value at such pressures is about 0.022, which is very low. The EMA does not usually provide accurate predictions for such low-porosity materials. But the decline in the porosity is only one aspect of the problem. The other, more important, aspect is how the porosity is distributed in the porous medium, as well as the grains' chemical composition. This point is well demonstrated by the data for Fahler 189. Even though its porosity is very low, the predictions are still accurate.

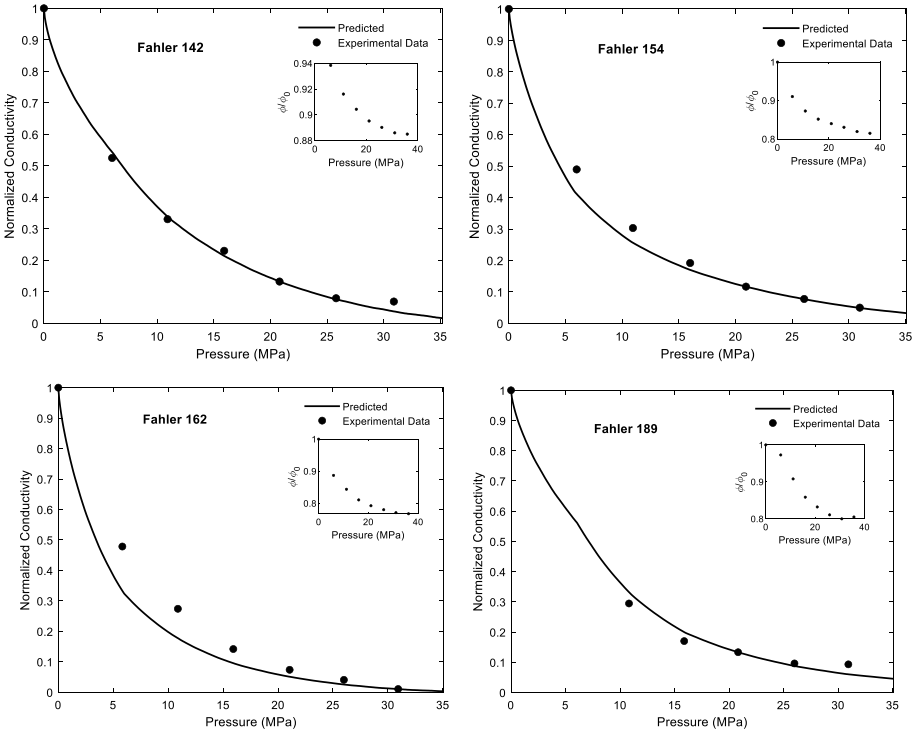

Fig. 7 Comparison of the predicted conductivities with the experimental data for the four Fahler sandstones

Fahler 162 is a fine-to-medium grained sandstone that consists of 46 percent quartz, 8 percent various lithics, and 6 percent chert, with the rest being other types of rock materials. Its cement contains 25 percent quartz overgrowth, 8 percent Fe oxide, and 8 percent clay. On the other hand, Fahler 189 is a medium-grained sandstone with 27 percent quartz, 27 percent chert, 11 percent various lithics, and 3 percent feldspar, with its cement consisting of 13 percent quartz overgrowth, 9 percent carbonate, 4 percent chalcedony, and 2 percent clay. Thus, Fahler 162 contains far more quartz, an extremely hard material, than Fahler 189, implying that the mechanism of porosity reduction in the two sandstones may be different.

8.7 Indiana Dark Sandstone

Indiana dark DH sandstone, with DH indicating that the sample was taken after drilling horizontally (parallel to bedding), had a relatively high initial porosity of 0.27. Figure 8 compares the predictions with the experimental data of Yale (1984). The agreement is excellent over much of the pressure range, with the largest difference between the prediction and data being about 5 percent at the highest pressure.

Note, however, that, similar to the Beaver and Berea sandstones, there is a qualitative difference between the behavior of the conductivity of Indiana DH sandstone and its permeability counterpart, shown in Fig. 12 of Part I. In the case of the permeability, the agreement between the theoretical predictions and the data is excellent at all the pressures. Since the only difference between the two cases appears to be the contribution of the surface conductivity, the fact that the theory predicts a faster decay of the conductivity at the highest pressures may imply that the model does not account adequately for the effect of surface conduction.

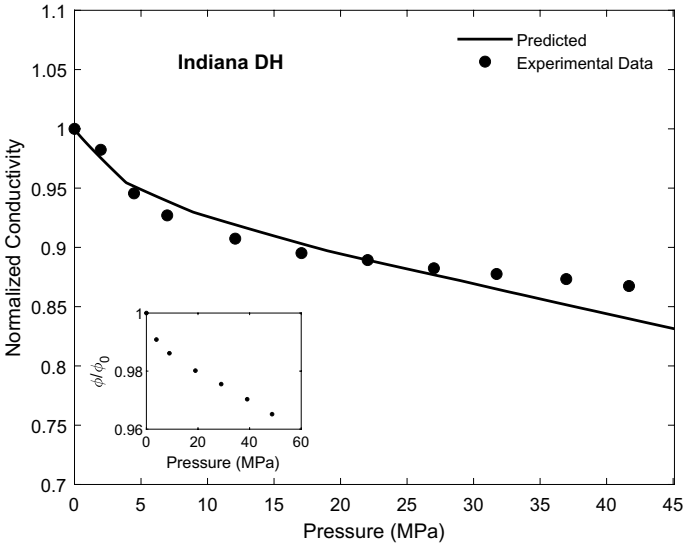

Fig. 8 Comparison of the predicted conductivities with the experimental data for the Indiana DH sandstone

8.8 Massillon Dark Sandstone

Massillon DH sandstone (from Massillon, Stark County, Ohio) is of quatzarenite type with an initial porosity of 0.161 and medium-size and well-sorted grains. Figure 9 compares the predictions with the experimental data of Yale (1984). Although the largest difference between the two sets is only about 3.5 percent at a pressure of 17.5 MPa, the trends in the two sets are somewhat different. The data indicate that the porosity at lower pressures reduced more strongly and, then, it leveled off, because 60 percent of the sandstone is quartz, which means it is difficult to reduce the porosity further even at 50 MPa. On the other hand, the EMA does not take into account the deformation mechanism and assumes simply that the porosity is reduced randomly.

8.9 Miocene Sandstone

The Miocene formation is a low-porosity sandstone of the feldspathic arenite type with an initial porosity of 0.083. It is known that due to high roundness and sorting of its grains, the sandstone contains long flow and transport paths over large distances (Saitoh and Masuda 2004). Figure 10 presents the comparison between the predictions with the pressure dependence of the electrical conductivity data of Yale (1984). The agreement is excellent. The well-connected and long transport and flow paths of the sandstone practically guarantee accurate predictions, because it is precisely under such conditions that the EMA is accurate.

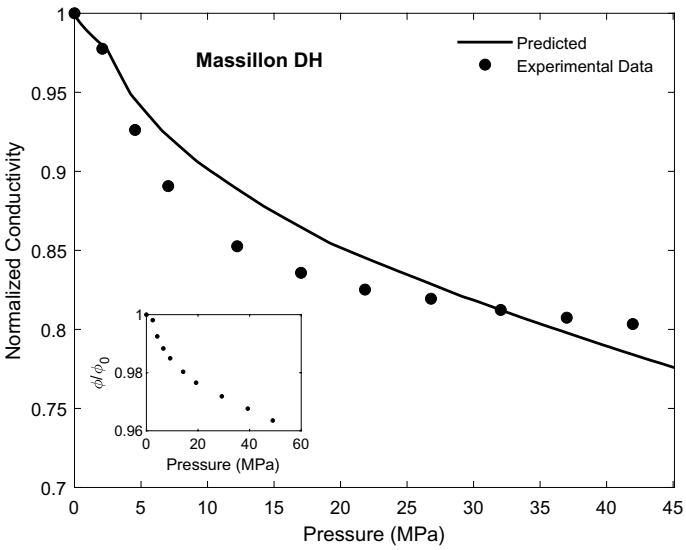

Fig. 9 Comparison of the predicted conductivities with the experimental data for the Massillon DH sandstone

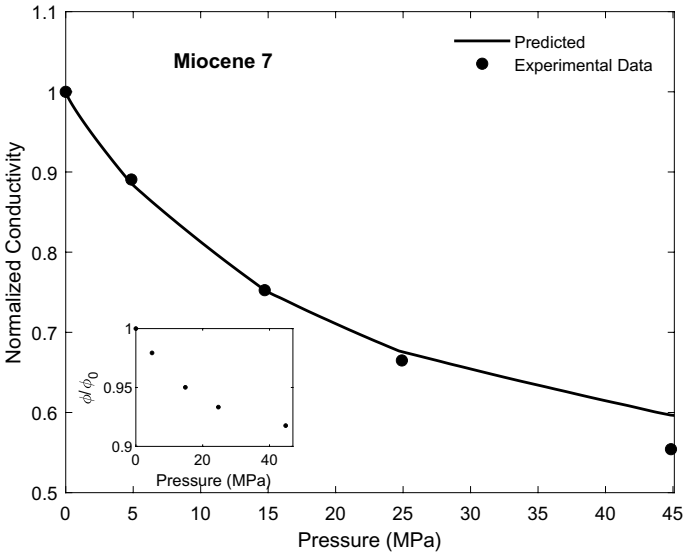

Fig. 10 Comparison of the predicted conductivities with the experimental data for the Miocene 7 sandstone

8.10 Pliocene Sandstone

Pliocene is the second and terminal epoch of Neogene period. The Pliocene formations are found in both marine form found in the Indian Ocean and western part of Yemen, and in the form of nonmarine sedimentary rock in the continental United States in, for example, Washington State (Walsh et al. 1987) and Oklahoma (Heran and et al. 2003). The initial porosity of the sample, referred to as Pliocene 35 by Yale (1984), was 0.2. Figure 11 compares the predictions with the data. The experimental data are somewhat scattered, but the largest difference between the data and predictions is about 9 percent at 25 MPa.

8.11 Tensleep Sandstone

Tensleep sandstone is from a geological formation in the entire Pennsylvanian sequence in central and northern Wyoming in the very early Permian age (Branson and Branson 1941) and represents crossbedded sandstone with thin limestone and dolomite beds (Kerr et al. 1986). The initial porosity of the sandstone was 0.146. In Fig. 12, we compare the predictions with the experimental data reported by Yale (1984). The agreement is very good over much of the range of the applied pressure. Note that after initially declining, the porosity remains unchanged over a range of pressure and then declines again, which explains the slower decline of the measured conductivity than the predictions at the highest pressures.

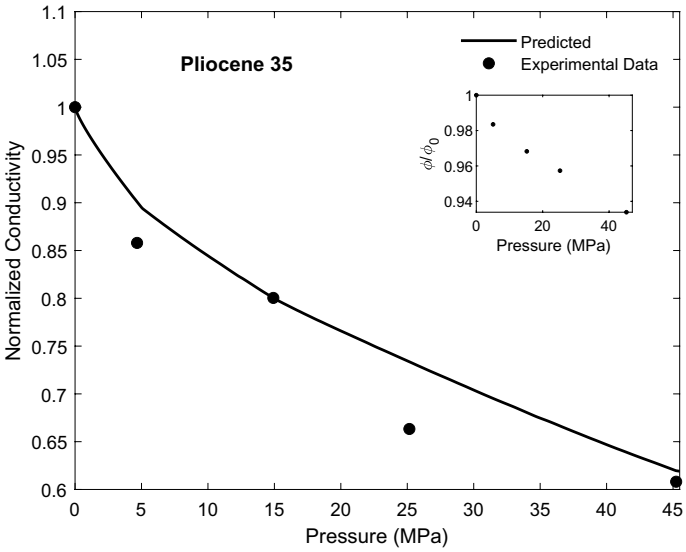

Fig. 11 Comparison of the predicted conductivities with the experimental data for the Pliocene 35 sandstone

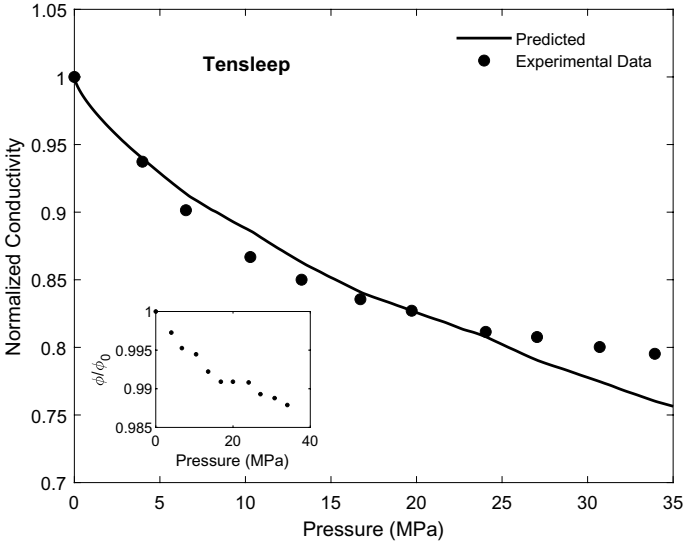

Fig. 12 Comparison of the predicted conductivities with the experimental data for the Tensleep 35 sandstone

8.12 Gulf Coast Sandstone

Yale (1984) referred to the sandstone as Tertiary 807. Tertiary rocks were formed during part of the Cenozoic era. The initial porosity of the sample was 0.22. Figure 13

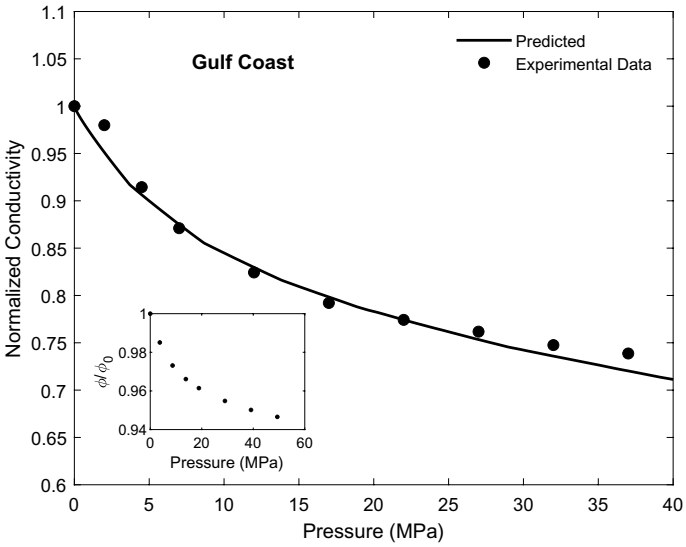

Fig. 13 Comparison of the predicted conductivities with the experimental data for the Tertiary 807 sandstone

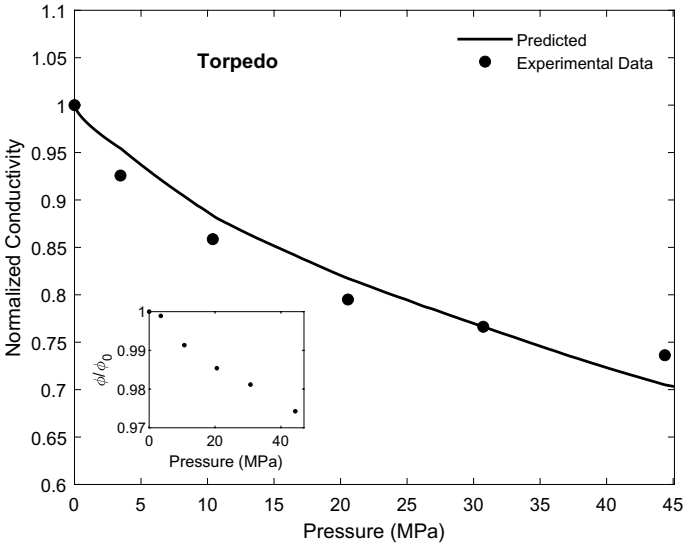

Fig. 14 Comparison of the predicted conductivities with the experimental data for the Torpedo sandstone

compares the theoretical predictions with the experimental data. The agreement between the predictions and the data is excellent.

8.13 Torpedo Sandstone

The Torpedo sandstone was from Kansas with an initial porosity of 0.202. As Fig. 14 indicates, the predicted electrical conductivity closely matches the measured data.

8.14 Triassic Sandstones

Triassic rocks were formed in the Triassic period, between 200 and 251 million years ago, with the morphology of such sandstones varying greatly, from very fine- to very coarse-grained. Although, generally speaking, they are porous formations with low- or ultra-low flow properties, they often have both tectonic and diagenetic fractures that provide flow paths. Yale (1984) reported the data for five samples of such sandstones, referred to as Triassic 26, 27, 34, 38, and 41, with their initial porosities being, respectively, 0.18, 0.18, 0.2, 0.2, and 0.21. Figure 15 compares the predictions for the conductivities with the experimental data. The agreement between the predictions and the data is uniformly very good for all samples.

8.15 Branford Sandstone

Figure 16 compares the predicted pressure dependence of the electrical conductivity of Branford (Connecticut) sandstone with the experimental data of Yale (1984). The initial porosity ϕ_0 of the sandstone, which is of sublitharenite type with medium-size and well-sorted grains made mostly of quartz, carbonate, and clay cement, is 0.11 (Bernabé 1989). Except for pressures $P > 30$ MPa, the agreement between the two is excellent. We shall return to the issue of the tail of the curve in Sect. 9.

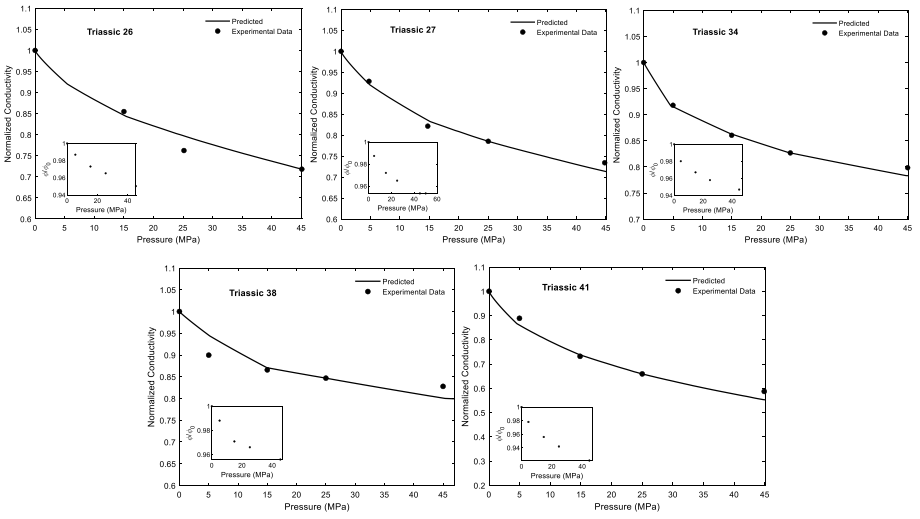

Fig. 15 Comparison of the predicted conductivities with the experimental data for the Triassic sandstone

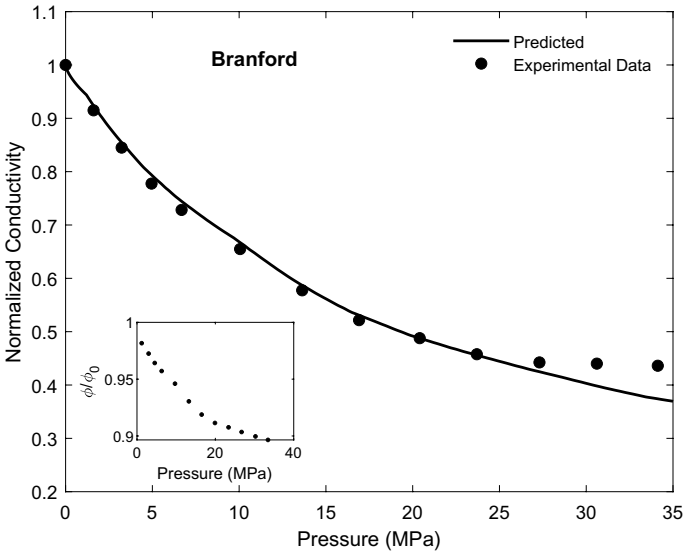

Fig. 16 Comparison of the predicted conductivities with the experimental data for the Branford sandstone

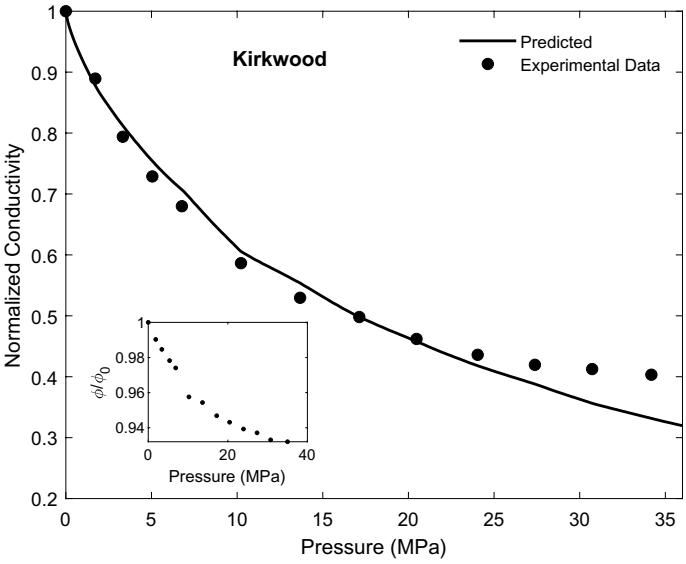

Fig. 17 Comparison of the predicted conductivities with the experimental data for the Kirkwood sandstone

8.16 Kirkwood Sandstone

Finally, we show in Fig. 17 the predictions for the conductivity of the Kirkwood sandstone and compare them with the data. The sandstone is a fairly clean orthoquartzite (Wyllie and Spangler 1952) with a porosity varying between 0.13 and 0.19. Once again, except for the

tail of the curve (to which we shall return in the next section), the agreement between the predictions and the data is essentially perfect, hence demonstrating the accuracy of the proposed model. Note that we showed in a previous paper (Richesson and Sahimi 2019) that the theory provides highly accurate predictions for the pressure dependence of the effective permeability of both Branford and Kirkwood sandstone.

9 Discussion

Several aspects of the predictions deserve to be considered in more details. In what follows, we discuss each aspect.

9.1 Limits of Accuracy of the Effective-Medium Approximation

The range of the validity of the EMA, as well as the MFA that we have developed for the deformation, are important issues. Sahimi (2003) and Hunt and Sahimi (2017) provide comprehensive discussions of the strengths and shortcomings of the EMA. As is well known, the EMA is (1) more accurate for two-dimensional (2D) media than for 3D, and (2) not very accurate in the *critical region*, i.e., the region near the critical porosity or the percolation threshold. In random media, the critical region is defined roughly by Sahimi (1994), $\phi - \phi_c \leq 1/Z$, where Z is the mean pore connectivity, and ϕc is the critical porosity. (3) If there are extended correlations between the pores' sizes, then the EMA is less accurate than in completely random porous media, although Mukhopadhyay and Sahimi (2000) suggested ways of taking into account the effect of such correlations.

9.2 The Reduction of the Conductivity at High Pressures

As described earlier, in some of the sandstones that we analyzed, the measured effective conductivity at high pressures decreases a bit more slowly than the theoretical predictions. One possible reason for this is that high pressures change the morphology of the porous media by mechanism(s) that the MFA and the EMA do not account for, such as opening up new cracks that provide new transport paths for the fluid and, hence, arrest to some extent the decline in the conductivity. Accounting for such effects would require modifications of the deformation theory that is beyond the scope of the present work. As discussed earlier, another possible reason for this behavior could be the inadequacy of the way we account for the effect of surface conduction.

9.3 Effect of the Boundary Conditions

We recall that deformation of geological formations is often caused by uniaxial stress, whereas in the experimental system and the present theoretical modeling the confining pressure is applied hydrostatically. Needless to say, the deformations that result from the two types of the boundary conditions are different, because the spatial distributions of the applied pressure in the two systems are different. But, when, for example, the overburden pressure exerts itself uniaxially in an oil reservoir, the surrounding rock limits the resulting lateral deformation. This implies that one obtains mostly vertical compaction, which represents smaller changes in the pore sizes than what is caused by hydrostatic pressure.

We already demonstrated that the theory provides accurate predictions for the macroscopic conductivity (and the permeability, as reported in Part I) as a function of the hydrostatic pressure that deforms the pore space much more extensively than a uniaxial stress would. Therefore, a slightly modified theory would be at least equally accurate for the case in which a uniaxial stress is exerted on a porous medium.

9.4 Effect of the Contact Law for the Grains

The theory that was developed in Part I and utilized in the present paper for determining the change in the size of a pore as a result of deforming a porous medium was based on the Hertz–Mindlin theory of contacting grains in unconsolidated porous media. The experimental data that were compared with the theoretical predictions were, however, for mostly consolidated sandstones that have been cemented. As shown by Dvorkin and Yin (1995), the cementation influences strongly the contact laws. This could provide an explanation as to why the fitted Young's moduli of various sandstones did not agree with what one might expect for such porous media, which contain a significant amount of quartz.

One way of addressing the theoretical shortcoming is to use the Hertz–Mindlin theory for cemented sandstones, rederive the expression for the change in the effective size of the pores, and recompute everything. An alternative, and perhaps simpler, approach would be to determine the change in the radius of a hollow cylinder (a pore throat), embedded in a solid material of a given Young's modulus, as a result of exposing the entire system to a hydrostatic pressure, which would indeed represent a mean-field approximation. The result can then be used to update the PSD for a given pressure and, hence, the effective conductivity. We will report on both approaches in a future paper.

10 Summary

This paper, the second a in series, presented a new theoretical approach for predicting the electrical conductivity σ_e of brine-saturated porous media that deform as a result of a hydrostatic pressure applied to them. The theory, a mean-field approximation, determines the change in the size of a pore between two grains that deform when the hydrostatic pressure is applied to them. Given the initial PSD of a porous medium before deformation, the Young's modulus, and the Poisson's ratio of the grains as the input, the theory determines the PSD of the pore space at pressure P. The updated PSD is used to determine the pore-conductance distribution, which is then used in the effective-medium approximation to predict the effective conductivity of the porous medium at the same pressure. Extensive comparison between the theoretical predictions and experimental data for the pressure dependence of σ_e of twenty-six sandstones indicated agreement between the two in almost all cases, ranging from very good to excellent.

The same type of approach can be used to estimate the effect of deformation on the dispersion coefficients in flow through deforming porous media. Work in this direction is in progress and will be reported in the future.

Acknowledgements S.R. is grateful to the Chevron Oil Company for a PhD scholarship. We are also grateful to the Petroleum Research Fund, administered by the American Chemical Society, and the National Science Foundation Grant CBET 2000968 for partial support of this work. We are also grateful to the anonymous reviewers whose critical comments and suggestions helped us improve the quality of the paper.

Funding Partial support of this work is by the Petroleum Research Fund, administered by the American Chemical Society, as well as be the National Science Foundation, and the National Science Foundation Grant CBET 2000968 for partial support of this work.

Availability of data and material The experimental data referenced and plotted throughout this work can be found from their respective published source that is listed in the reference section. For example, much of the data is acquired from Yale, D.P. 1984.

Code availability The code used to produce the figures is custom MATLAB code using simple numerical procedures described in the work.

Declarations

Conflicts of interest The authors declare that they have no conflict of interest.

References

Archie, G.E.: The electrical resistivity log as an aid in determining some reservoir characteristics. Pet. Trans. AIME **146**, 54 (1942)

Bernabé, Y.: Pore geometry and permeability modeling from pressure dependence of transport properties in sandstones (1989). https://dspace.mit.edu/bitstream/handle/1721.1/75148/1989.12

Blunt, M.J.: Multiphase Flow in Permeable Media: A Pore-Scale Perspective. Cambridge University Press, Cambridge (2017)

Branson, E.B., Branson, C.C.: Geology of the Wind River mountains. Wyoming Am. Asso. Pet. Geol. Bull. **25**, 120 (1941)

Cai, J., Wei, W., Hua, X., Wood, R.A.: Electrical conductivity models in saturated porous media: a review. Earth Sci. Rev. **171**, 419 (2017)

Cheung, C.S.N., Baud, P., Wong, T.-F.: Effect of grain size distribution on the development of compaction localization in porous sandstone. Water Res. Res. **39**, L21302 (2012)

Clavier, C., Coates, G., Dumanoir, J.: Theoretical and experimental bases for the dual-water model for interpretation of shaly sands. Soc. Pet. Eng. J. **24**, 153 (1984)

Crook, N., Binley, A., Knight, R., Robinson, D.A., Zarnetske, J., Haggerty, R.: Electrical resistivity imaging of the architecture of substream sediments. Water Resour. Res. **44**, W00D13 (2008)

Daigle, H., Ghanbarian, B., Henry, P., Conin, M.: Universal scaling of the formation factor in clays: example from the Nankai Trough. J. Geophys. Res. Solid Earth **120**, 7361 (2015)

Dashtian, H., Yang, Y., Sahimi, M.: Non-universality of the Archie exponent due to multifractality of the resistivity well logs. Geophys. Res. Lett. **42**, 10655 (2015)

David, C., Gueguen, Y., Pampoukis, G.: Effective medium theory and network theory applied to the transport properties of rock. J. Geophys. Res. **95**(B5), 6993 (1990)

Doyen, P.M.: Permeability, conductivity, and pore geometry of sandstone. J. Geophys. Res. **93**(B7), 7729 (1988)

Dvorkin, J., Yin, H.: Contact laws for cemented grains: implications for grain and cement failure. Int. J. Solids Struct. **32**, 2497 (1995)

Farid, M.F., Arns, J.-Y., Pinczewski, W.V., Arns, C.H.: Experimental and numerical investigation on stress dependence of sandstone electrical properties and deviations from Archie's law. Paper presented at the SPE Annual Technical Conference and Exhibition, Dubai, U.A.E. (2016)

Fredrich, J. T., Greaves, K. H., Martin, J. W.: Pore geometry and transport properties of Fontainebleau sandstone. Int. J. Rock Mech. Mining Sci. Geomech. Abst. **30**, 691 (1993)

Ghanbarian, B., Berg, C.F.: Formation factor in Bentheimer and Fontainebleau sandstones: Theory compared with pore-scale numerical simulations. Adv. Water Resour. **107**, 139 (2017)

Ghanbarian-Alavijeh, B., Hunt, A.G., Ewing, R.E., Sahimi, M.: Tortuosity in porous media: a critical review. Soil Sci. Soc. Am. J. **77**, 1461 (2013)

Ghanbarian, B., Hunt, A.G., Ewing, R.P., Skinner, T.E.: Universal scaling of the formation factor in porous media derived by combining percolation and effective medium theories. Geophys. Res. Lett. **41**, 3884 (2014)

Heran, W.D., Green, G., Stoeser, D.B.: A digital geologic map database of Oklahoma: USGS Open File Report 03-247, scale 1:250,000 (2003)

Hertz, H. R.: Ueber die Berührung fester elastischer Körper. J. für die reine und angewandte Mathematik (Crelle's Journal) **92**, 156 (1882)
Hunt, A.G., Sahimi, M.: Flow, transport, and reaction in porous media: Percolation scaling, critical-path analysis, and effective-medium approximation. Rev. Geophys. **55**, 993 (2017)
Karger, J., Pfeifer, H., Heink, W.: The propagator representation of molecular transport in microporous crystallites. In: Waugh, J.S. (eds.) Advances in Magnetic Resonance, vol. 12, p. 1. Academic Press, San Diego (1981)
Kerr, D.R., Wheeler, D.M., Rittersbacher, D.J., Home, J.C.: Stratigraphy and sedimentology of the Tensleep sandstone (Pennsylvanian and Permian), Bighorn Mountains. Wyoming Earth Sci. Bull. **19**, 61 (1986)
Lindquist, W.B., Venkatarangan, A., Dunsmuir, J., Wong, T.-F.: Pore and throat size distributions measured from synchrotron X-ray tomographic images of Fontainebleau sandstones. J. Geophys. Res. **105**, 509 (2000)
Lyklema, J.: Fundamentals of Interface and Colloid Science, vol. 1. Academic Press, London (1993)
Mindlin, R.D.: Compliance of elastic bodies in contact. J. Appl. Mech. **16**, 259 (1949)
Mitra, P.P., Sen, P.N.: Effects of microgeometry and surface relaxation on NMR pulsed-field-gradient experiments: simple pore geometries. Phys. Rev. B **45**, 143 (1992)
Mitra, P.P., Sen, P.N., Schwartz, L.M., Le. Doussal, P.: Diffusion propagator as a probe of the structure of porous media. Phys. Rev. Lett. **24**, 3555 (1992)
Mitra, P.P., Sen, P.N., Schwartz, L.M.: Short-time behavior of the diffusion coefficient as a geometrical probe of porous media. Phys. Rev. B **47**, 8565 (1993)
Mukhopadhyay, S., Sahimi, M.: Calculation of the effective permeabilities of field-scale porous media. Chem. Eng. Sci. **55**, 4495 (2000)
Odagaki, T., Lax, M.: Coherent-medium approximation in the stochastic transport theory of random media. Phys. Rev. B **24**, 5284 (1981)
Rassamdana, H., Dabir, B., Nematy, M., Farhani, M., Sahimi, M.: Asphalt flocculation and deposition: I. The onset of precipitation. AIChE J. **42**, 10 (1996)
Revil, A., Cathles III, L.M., Losh, S., Nunn, J.A.: Electrical conductivity in shaly sands with geophysical applications. J. Geophys. Res. **B103**, 23925 (1998)
Revil, A., Ghorbani, A., Mapeli, C., Livo, K., Prasad, M.: Differential pressure dependence of the complex conductivity of sandstones. Geophys. J. Int. **219**, 2110 (2019)
Richesson, S., Sahimi, M.: Hertz-Mindlin theory of contacting grains and the effective-medium approximation for the permeability of deforming porous media. Geophys. Res. Lett. **46**, 8039 (2019)
Richesson, S., Sahimi, M.: Flow and transport properties of deforming porous media. I. Permeability. Transp. Porous Media (under review)
Sahimi, M.: Applications of Percolation Theory. Taylor and Francis, London (1994)
Sahimi, M.: Heterogeneous Materials I: Linear Transport and Optical Properties, chap. 5. Springer, Berlin (2003)
Sahimi, M.: Flow and Transport in Porous Media and Fractured Rock, 2nd edn. Wiley-VCH, Weinheim (2011)
Sahimi, M., Hughes, B.D., Scriven, L.E., Davis, H.T.: Stochastic transport in disordered systems. J. Chem. Phys. **78**, 6849 (1983)
Saitoh, Y., Masuda, F.: Miocene sandstone of 'continental' origin on Iriomote Island, southwest Ryukyu Arc. Eastern Asia. J. Asian Earth Sci. **24**, 137 (2004)
Stejskal, E.O., Tanner, J.E.: Spin diffusion measurements: spin echoes in the presence of a time-dependent field gradient. J. Phys. Chem. **67**, 288 (1965)
Stern, O.: Zur Theorie der Elektrolytischen Doppelschicht. Zeitschrift für Elektrochemie **30**, 508 (1924)
Stroud, D.: Generalized effective-medium approach to the conductivity of inhomogeneous materials. Phys. Rev. B **12**, 3368 (1975)
Vanderborght, J., Kemna, A., Hardelauf, H., Vereecken, H.: Potential of electrical resistivity tomography to infer aquifer transport characteristics from tracer studies: a synthetic case study. Water Resour. Res. **41**, W06013 (2005)
Wyble, D.O.: Effect of applied pressure on the conductivity, porosity and permeability of sandstones. Trans. AIME **213**, 430 (1958)
Walsh, T.J., Korosec, M.A., Phillips, W.M., Logan, R.T., Schasse, H.W.: Geologic map of Washington-Southwest quadrant: Washington Division of Geology and Earth Resources, Geologic Map GM-34, scale 1:250,000 (1987)
Waxman, M.H., Smits, L.J.M.: Electrical conductivities in oil-bearing shaly sands. Soc. Pet. Eng. J. **8**, 107 (1968)

Woessner, D.E.: NMR spin-echo self-diffusion measurements on fluids undergoing restricted diffusion. J. Phys. Chem. **67**, 1365 (1963)
Woodruff, W.F., Revil, A., Prasad, M., Torres-Verdín, C.: Measurements of elastic and electrical properties of an unconventional organic shale under differential loading. Geophysics **80**, D363 (2015)
Wyllie, M.R.J., Spangler, M.B.: Application of electrical resistivity measurements to problem of fluid flow in porous media. AAPG Bull. **36**, 352 (1952)
Yale, D.P.: Network Model of Flow, Storage and Deformation in Porous Rocks. Ph.D. Dissertation, Stanford University, Stanford, California (1984)